

---

## **Constrained Solid-State Foaming of Microcellular Panels**

Krishna Nadella\*, Vipin Kumar and Wei Li

Department of Mechanical Engineering, University of Washington, Seattle, WA 98195-2600, USA

**Received: 16 December 2004 Accepted: 29 March 2005**

### **ABSTRACT**

*This paper presents a novel constrained foaming process to produce microcellular panels. A systematic study of various process variables is conducted using a two-stage, sliding-level design of experiment approach. The resulting microcellular sheets have thicknesses in the 5 – 15 mm range and densities reductions as low as 92%. It is shown that an unfoamed integral skin of desired thickness can be produced with a microcellular core at various densities. These microcellular panels are envisioned for use in advanced panel systems and sandwich structures, such as in housing construction and other load-bearing applications.*

### **1. INTRODUCTION**

Microcellular plastics refer to closed-cell thermoplastic foams with a very large number of very small bubbles. Typically, the cells are on the order of 10  $\mu\text{m}$  in diameter and there are  $10^8$  or more cells per cubic centimeter ( $\text{cm}^3$ ) of the foam. The idea to introduce such small bubbles in plastics was first introduced by Martini *et al*<sup>(1)</sup> as a means to reduce the density of solid plastics, thus saving on material costs in applications where the full mechanical properties of solid plastics were not needed. The applications envisioned were primarily for the packaging industry with a typical wall thickness in the range of 0.5 to 1.5 mm. An early review of microcellular plastics can be found in Kumar<sup>(2)</sup>.

Being foam materials, microcellular polymers have inherited beneficial characteristics such as lightweight and low thermal conductivity. Mechanical properties of several microcellular polymers have been reported. The tensile strength of microcellular polymers has been found to be proportional to the foam relative density (ratio of density of foam to the density of solid polymer)<sup>(3)</sup>. The fatigue life of microcellular PC of above 90% relative density is reported to be as much as four times that of the solid PC<sup>(4)</sup>. The impact

---

\*Corresponding author email: krivenk@u.washington.edu

strength of microcellular PC of relative density 60% and above was found to be greater than that of solid PC<sup>(5,6)</sup>. For microcellular CPET with density reductions of up to 50% of the solid polymer, the impact strength was found to be comparable to the solid polymer<sup>(7)</sup>. However, for microcellular PVC the impact strength decreased linearly with the relative density<sup>(8)</sup>. The thermal conductivity of microcellular CPET foams decreases linearly with increasing void fraction<sup>(9)</sup>. These characteristics of microcellular polymers combined with the smooth integral skin render microcellular foams a novel class of engineering materials.

The basic solid-state microcellular process is a two-stage batch process. In the first stage, the polymer is placed in a pressure vessel with a high-pressure non-reacting gas. Over time, the gas diffuses into the polymer, and attains a uniform concentration throughout the polymer specimen. When this specimen is removed from the pressure vessel and brought to the atmospheric pressure, a “supersaturated” specimen that is thermodynamically unstable is produced due to the excessive gas dissolved into the polymer. The gas pressure to which the polymer sample is exposed to in the vessel is termed saturation pressure ( $P_{\text{sat}}$ ). The temperature inside the pressure vessel during saturation is called saturation temperature ( $T_{\text{sat}}$ ).  $T_{\text{sat}}$  is usually equal to the room temperature. In the second stage, the specimen is heated to what is termed the foaming temperature ( $T_{\text{foam}}$ ). This step is typically carried out in a heated liquid bath with temperature control. The dissolved gas lowers the glass transition temperature ( $T_g$ ) of the polymer<sup>(10)</sup> and the foaming temperature only needs to be slightly above the glass transition temperature of the polymer-gas system in order for the bubbles to nucleate and grow.

During the transfer of the supersaturated specimen from the pressure vessel to the heated bath, the dissolved  $\text{CO}_2$  gas diffuses out of the surfaces of the specimen to the atmosphere. This phenomenon is termed “desorption” and the time elapsed between the instant the pressure vessel is vented to the instant the gas saturated specimen is introduced into the heated liquid bath is called desorption time ( $t_d$ ). The diffusion of gas outwards from the specimen’s surface is primarily driven by the gas concentration gradient between the specimen and the atmosphere. With a sufficiently long desorption time the gas concentration in the surface layer drops below the minimum concentration needed for bubble nucleation. The most significant result of this phenomenon is the appearance of a smooth unfoamed integral skin on the microcellular core<sup>(11)</sup>. The thickness of the integral skin increases with desorption time and can be easily controlled.

Earlier, Baldwin *et al*<sup>(12,13)</sup> demonstrated an extrusion process to produce microcellular sheets. In the extrusion process supercritical carbon dioxide is

injected into the molten polymer inside the extruder barrel to form a two phase mixture. Gas diffusion into the polymer matrix is enabled using a diffusion enhancing device, such as a static mixing element. Once a single phase uniform polymer-gas solution is formed the molten polymer is passed through a nucleating nozzle followed by a shaping die. Production speed is the primary advantage of using extrusion for producing flat microcellular panels. The disadvantage of extrusion is that an integral skin is very difficult to create.

Initial attempts to produce microcellular sheets (thickness > 3 mm) using the conventional solid-state microcellular process have resulted in specimens (thickness > 6 mm) that are curved and grossly distorted<sup>(14)</sup>. The constrained foaming technology proposed in this paper controls the foam growth process in the thickness direction. It is capable of creating microcellular panels with integral skins of desirable thickness, reducing bulk density and thermal conductivity while increasing their specific strength. These materials have the potential to become new, lightweight building blocks for future house construction and other load-bearing applications.

## 2. THE PROPOSED CONSTRAINED FOAMING PROCESS

Figure 1 shows a schematic of the proposed constrained foaming process. It is a scaled-up version of the basic two-stage batch microcellular process. In the first stage diffusion of the CO<sub>2</sub> gas into the solid polymer sheet occurs in a high pressure environment similar to the conventional batch process<sup>(15-17)</sup>. Once the polymeric sheet attains an equilibrium gas concentration through

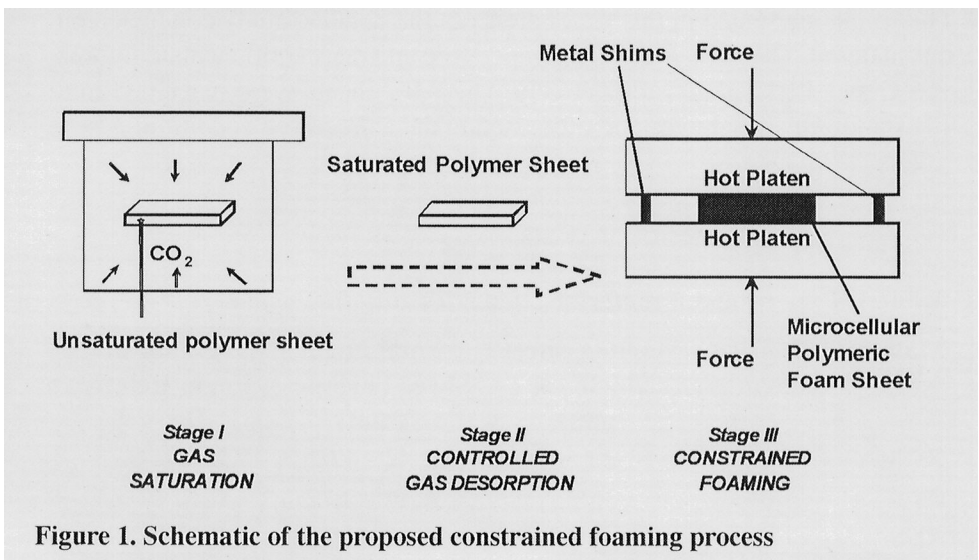


Figure 1. Schematic of the proposed constrained foaming process

the thickness, the sheet is removed from the pressure vessel and is exposed to the atmospheric pressure for a predetermined length of time, called desorption time ( $t_d$ ). Desorption time is used as a process variable to achieve the desired integral skin thickness. In the final stage the gas-laden polymeric sheet is foamed between the heated platens of a hydraulic press. The gap between the platens is controlled by use of metal shims of thickness equal to the desired foam thickness. A large force is applied on the platen to keep the gap constant so as to produce a flat microcellular panel of uniform thickness. The foaming process is thus constrained to conform to the flat geometry with a preset thickness. In a variation of this process the platens can be replaced by surfaces of a mold to create desired shapes other than a flat geometry. The primary advantage of using the constrained foaming process is that flat sheets of microcellular plastics can be produced. In addition, it is easy to create an integral skin of desired thickness by using desorption time as a process variable. As desorption time increases the thickness of the integral skin increases.

### 3. EXPERIMENTAL

#### 3.1. Materials

PMMA, PS and ABS sheets were used in this study. PMMA and PS sheets were supplied by Aluisse Technology and Management, Inc., Switzerland. The ABS sheets were GE's Cyclicolac HXW Extrusion Grade. Table 1 lists the basic information on these materials. Of these three materials a detailed study of the process variables was conducted on GE's HXW Grade ABS material. The results presented in this paper are from the detailed study conducted on this material. The glass transition temperature and density of the material was 116 C and 1.037 g/cm<sup>3</sup>, respectively. The ABS sheets were machined into 101.6 mm square samples and processed in the as-received condition.

Table 1. Experimental materials, densities and dimensions

Material	Density (g/cm <sup>3</sup> )	Starting Sheet Thickness (mm)	Final Foam Sheet Thickness (mm)	Range of Foam Relative Density
PMMA	1.193	2.55	3.42 - 4.02	0.23 - 0.75
PS	1.073	3.02	4.64 - 4.72	0.10 - 0.85
ABS	1.037	4.75, 9.53	4.82 - 15.125	0.10 - 0.98

### 3.2. Equipment

For the gas saturation step, the ABS square samples were placed in a 0.28 m diameter and 0.635 m long pressure vessel. The pressure vessel, made by Ken-Weld Co. Inc, is rated for use up to a maximum pressure of 10.34 MPa at 0 °C. The pressure inside the vessel was regulated using an OMEGA CN8500 process controller with a resolution of  $\pm 0.01$  MPa. A Mettler-Toledo AE240 precision balance with an accuracy of 10  $\mu\text{g}$  was used to measure the gas solubility in solid ABS during saturation. The same balance was used to measure the density of microcellular ABS samples as described in the experimental procedure section. The constrained foaming step was carried out on an MTP-14 hydraulic press with heated platens. The press was made by Tetrahedron Associates, Inc. and is rated for use up to a maximum force of 50 tons. To create a gap between the top and bottom platens, two stacks of metal shims each with a stacked height of 13 mm were used. The microstructure characterization of the microcellular ABS samples was conducted using a FEI Siron XL 30 scanning electron microscope (SEM).

### 3.3. Experimental Design

The variables of the constrained foaming process were examined in order to determine a potentially significant set for detailed study. As summarized in Table 2, high and low priorities were assigned to the process variables based on previous experience and published data on the ABS-CO<sub>2</sub> system<sup>(17)</sup>. The

**Table 2. Variable that could affect the quality of thick microcellular sheet foaming process**

S. No	Parameters	Priority
1	Saturation pressure	High
2	Temperature of platens (Foaming temperature)	High
3	Desorption time	High
4	Thickness of starting material	High
5	Force exerted by the platens	Low
6	Foaming time	Low
7	Shim thickness	Low
8	Environmental temperature during desorption	Low
9	Environmental pressure during desorption	Low
10	Composition of raw material	Low
11	Saturation temperature	Low
12	Humidity of the environment	Low

first four variables in the table were chosen as high priority variables for a systematic study. The solid-state microcellular process is complicated due to interdependency among the process variables. For example, according to data reported by Murray *et al*<sup>(17)</sup>, to obtain a foamed structure of desired density in ABS the foaming temperature and saturation pressure have to be varied together to reach suitable process conditions. This interdependency can be observed in Figure 2. In general, if the saturation pressure is low, the foaming temperature has to be high to achieve the same bulk density for the final product. In addition, without a foamed structure, the experiment does not provide useful information on bulk density and skin thickness. Therefore, conventional design of experiment, in which the settings of process variables are independently chosen, does not provide an efficient experiment plan, because they result in data points outside of the interest area or considerably smaller response area to be explored.

In this study, a two-stage, sliding-level design of experiment approach<sup>(18)</sup> was used to resolve the parameter interdependency problem. The foaming temperature was chosen as a “slid factor” whose settings were determined based on those of other variables.

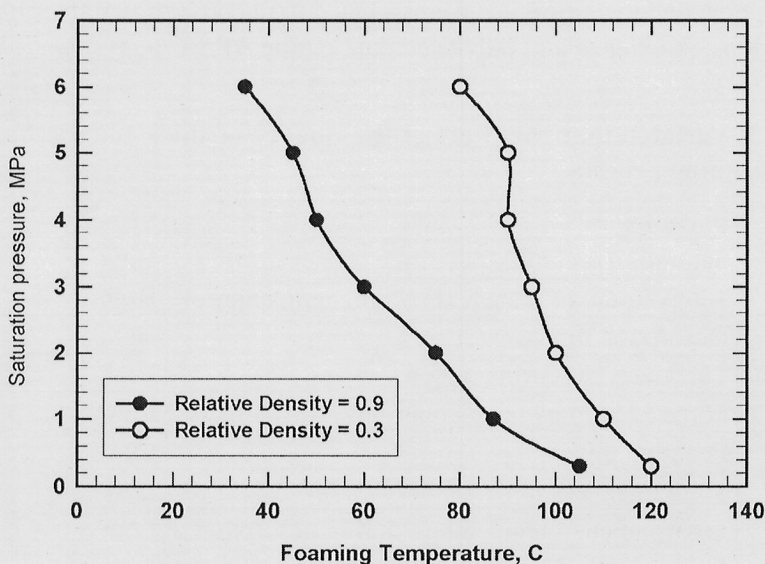


Figure 2. The interdependency between foaming temperature and saturation pressure. Thus a foam of 0.3 relative density can be produced, for example, at (6 MPa, 85 °C) or at (1 MPa, 110 °C)

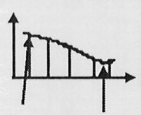
Table 3 shows the settings of the process variables. The saturation pressure and desorption time were chosen as three-level variables, and the starting thickness of the unfoamed sheet as a two-level variable. The foaming temperatures were determined for each of the combinations of the other factors' levels.

As shown in Table 4, given any setting of the other three variables, the maximum and minimum foaming temperatures had to be found first. These two temperatures would yield the maximum and minimum possible relative density for different pressures. For ABS the minimum foaming temperature for a given saturation pressure was experimentally determined by Murray *et al*<sup>(17)</sup>. Alternatively, this minimum foaming temperature could be estimated by using Chow's model<sup>(19)</sup>. The maximum foaming temperature, on the other hand, is not easy to find. Fortunately, prior experience can help with the search. For example, the maximum foaming temperature is known to be close to the glass

**Table 3. Selected experimental factors and their levels**

Factors	Levels		
	1	2	3
Saturation Pressure	1 MPa	3 MPa	5 MPa
Desorption Time	0 day	1 day	2 days
Starting Thickness of Unfoamed Sheet	4.75 mm	9.53 mm	--
Foaming Temperature (Temperature of Platens)	Five levels of foaming temperature at each combination of factor levels in the matrix for the above three factors		

**Table 4. Design matrix of the experiment.  $P_{sat}$  is saturation pressure,  $t_d$  is desorption time,  $h$  is starting thickness,  $T_{foam}$  is foaming temperature, and  $\rho_{rel}$  is relative density**

$P_{sat}$	$t_d$	$h$	$T_{foam}$	$\rho_{rel}$
1	1	1	$T_{11} T_{12} T_{13} T_{14} T_{15}$	 <p>Min Foaming Temperature</p> <p>Lowest relative density will be explored</p>
1	2	1	$T_{21} T_{22} T_{23} T_{24} T_{25}$	
1	3	1	$T_{31} T_{32} T_{33} T_{34} T_{35}$	
1	1	2	$T_{41} T_{42} T_{43} T_{44} T_{45}$	
...	...	...	...	

transition temperature,  $T_g$  of unsaturated ABS. It decreases as the saturation pressure increases. Once the maximum foaming temperature was determined, another three levels of temperature were chosen equally spaced within the two extreme temperatures. Based on the above design, the total number of experiments conducted was  $3 \times 3 \times 2 \times 5 = 90$ .

### 3.4. Experimental Procedure

For gas saturation, thirty ABS square samples were interleaved with porous paper towel and then placed in the pressure vessel which was then filled with  $\text{CO}_2$  gas at 5 MPa and room temperature (22 °C). The saturation pressure and saturation temperature were regulated to  $\pm 0.1$  MPa and  $\pm 1$  °C, respectively. After the ABS samples achieved uniform gas concentration across the thickness the pressure vessel was vented and the samples were removed. This procedure was repeated for saturating another thirty sheets each at 3 MPa and 1 MPa. For each of the 90 experiments the ABS sheets were allowed to desorb  $\text{CO}_2$  gas at atmospheric conditions for 0 day, 1 day or 2 days, as outlined in Table 4.

For the foaming step the platens were preheated to the desired foaming temperature and were separated by metal shims to create a gap of 13 mm between them. The shim thickness was determined based on the final desired thickness of the microcellular sheets. Once the preset desorption time had elapsed the gas-laden ABS samples were transferred into this gap as shown in Figure 1. After insertion in the heated press a normal force of 3629 kg (4 tons) was applied by the platens on the top and bottom surfaces of the polymer sheet to constrain its growth in the thickness direction while foaming. The foaming cycle of the saturated ABS samples consisted of two steps, the heating (or foam growth) step and cooling (or foam stabilization) step. During the heating step the platens were maintained at the desired foaming temperature for 600 s. This was done to ensure that the center of the specimen reached the desired foaming temperature and to allow enough time for the maximum possible foam growth that can occur at this temperature. In the cooling step the platens were cooled down to room temperature (22 °C) for 600 s under the same force as when heating. This was to stabilize the foam structure and ensure that the microcellular polymer sheet reached room temperature thereby preventing any gross distortion upon removal from the press. The search for the maximum foaming temperatures for ABS during the constrained foaming process was also based on the batch microcellular process data for the same material as reported by Murray *et al*<sup>17</sup>. Compared to the batch data the foaming temperatures used in this study were set higher in order to adjust for the longer desorption times of 24 hours and 48 hours. The foaming temperatures used were in the range of 40 °C – 140 °C.



After foaming in the press, the microcellular ABS sheets were allowed to age at the atmospheric pressure and room temperature for 168 h so that any remaining dissolved gas diffuses out. The densities of the microcellular sheets were then determined using the ASTM D792-91 standard test method<sup>(20)</sup>. The samples used for density measurement were approximately 25 mm x 25 mm and were cut out from the flat foamed square samples. Selected foams were subjected to microstructure investigation primarily to characterize the skin thickness. The samples were selected based on their final density and processing conditions. The procedure includes freeze fracturing to obtain a clean brittle fractured surface, sputter coating the clean surface with Au-Pd to make it conductive, and finally performing microstructure investigation using the SEM.

#### 4. RESULTS AND DISCUSSION

##### 4.1. CO<sub>2</sub> Sorption in ABS

Figure 3 shows the sorption curves at 3 MPa and 5 MPa for the ABS sheets of two thicknesses. The 4.75 mm thick samples saturate in approximately 350 h at 3 MPa, while at 5 MPa the saturation takes only 100 h. The 9.53 mm thick samples require 600 h and 300 h to saturate at 3 MPa and 5 MPa, respectively. It is

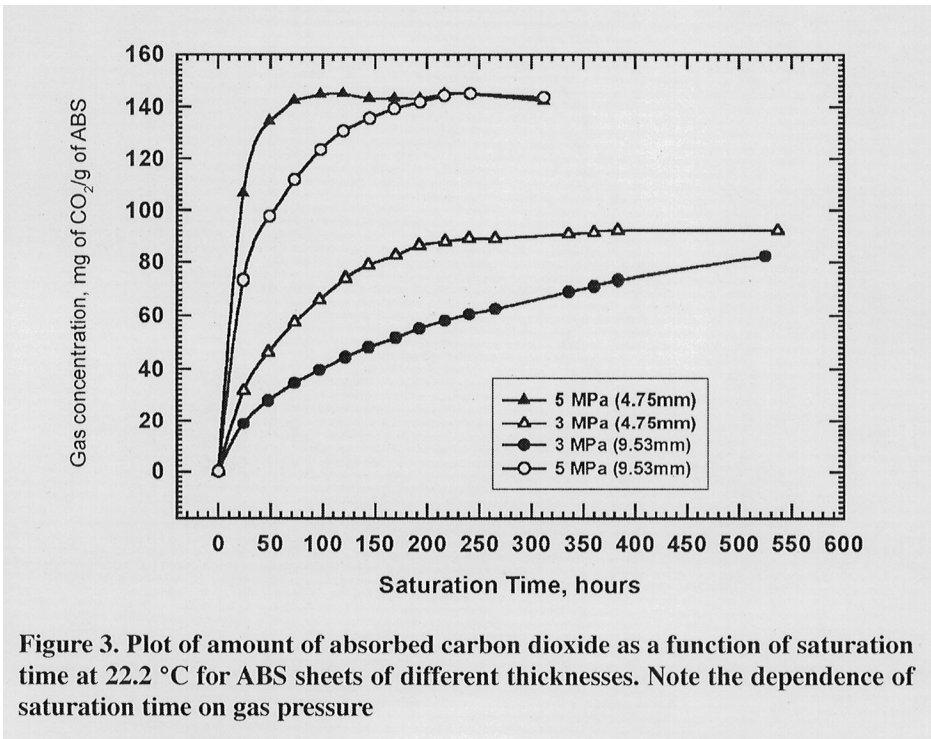


Figure 3. Plot of amount of absorbed carbon dioxide as a function of saturation time at 22.2 °C for ABS sheets of different thicknesses. Note the dependence of saturation time on gas pressure

evident from these sorption curves that diffusion of  $\text{CO}_2$  in ABS is concentration dependent. For a given sample thickness, as the saturation pressure increases the time required to reach equilibrium gas concentration decreases for ABS. This is in contrast to polymer gas systems such as PC- $\text{CO}_2$  and PVC- $\text{CO}_2$ , in which diffusion is independent of gas concentration<sup>(15,16)</sup>. Figure 4 shows the sorption curves for the ABS- $\text{CO}_2$  system normalized for thickness. It can be seen that before reaching the equilibrium gas solubility, the 9.53 mm thick samples have higher gas concentration than the 4.75 mm thick samples. This can be attributed to larger surface area available for gas diffusion in the thicker samples compared to the thinner samples. The 9.53 mm thick samples used in this study have a 13.5% larger surface area than the 4.75 mm thick samples.

#### 4.2. ABS- $\text{CO}_2$ Process Space

Figure 5 shows a photograph of 6 mm thick microcellular ABS sheets produced using the constrained foaming process depicted in Figure 1. Figures 6 and 7 show the plots of relative density *versus* foaming temperature for microcellular ABS sheets produced using the constrained foaming process from starting thicknesses of 9.53 mm and 4.75 mm respectively. Relative density is defined as the ratio of density of the foam to that of the solid. In general, these curves

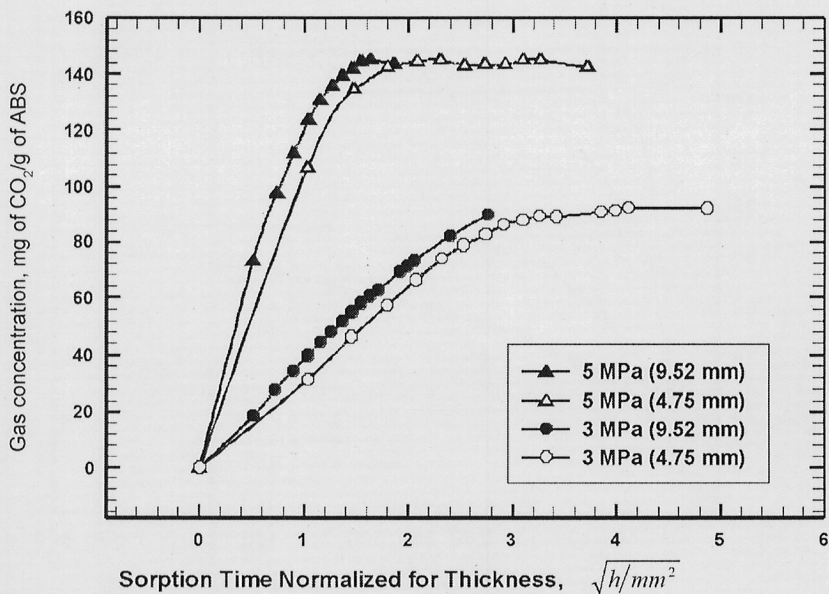


Figure 4. Sorption plots at 3 MPa and 5 MPa for ABS- $\text{CO}_2$  system at 22.2 °C, normalized for sample thickness

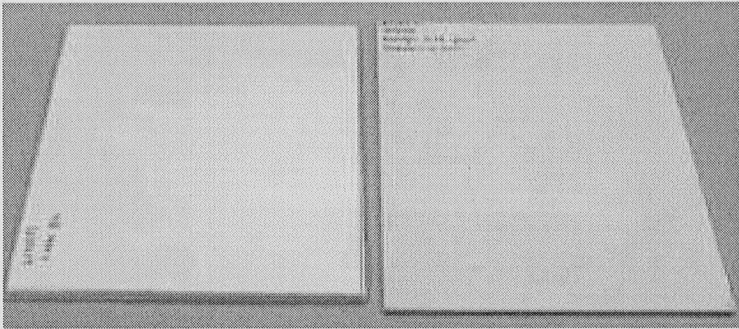


Figure 5. Photograph of 6 mm thick microcellular ABS specimens produced in the constrained foaming process. Note the flat geometry resulting from constraining foam growth in the thickness direction

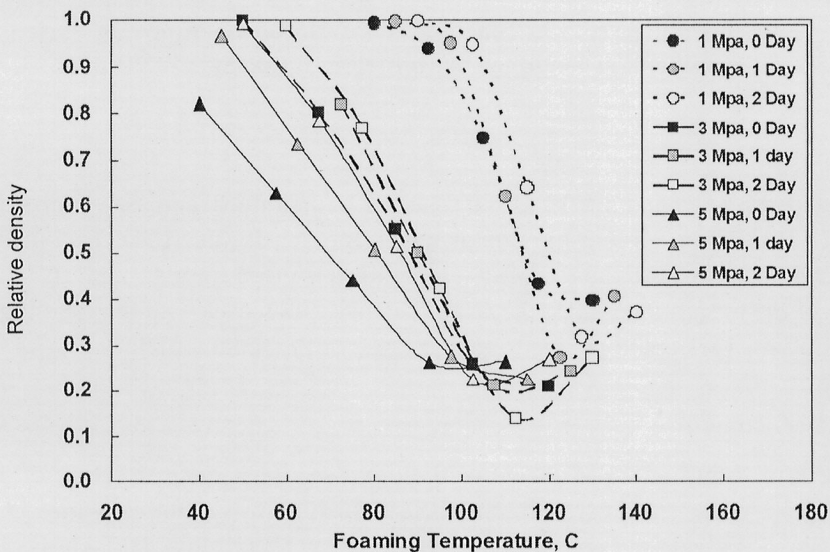
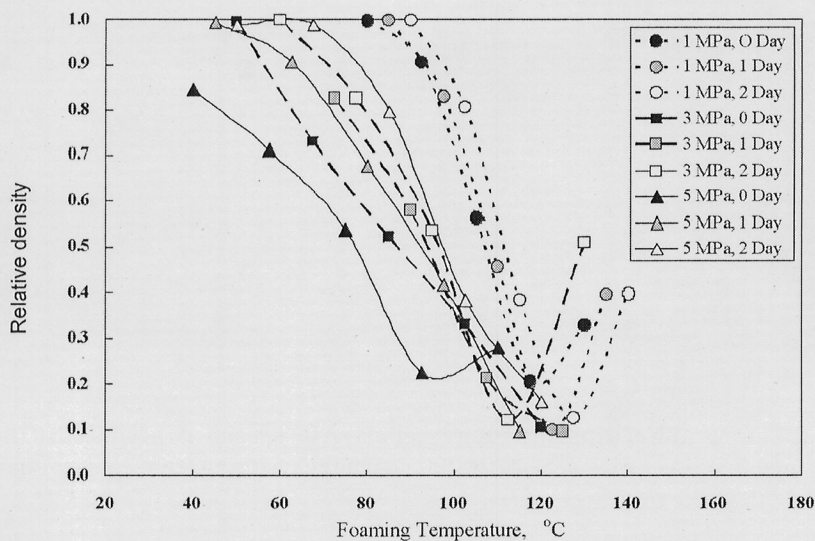


Figure 6. Relative density as a function of foaming temperature at various saturation and desorption conditions for initial sheet thickness 9.53 mm

reveal that samples saturated at higher pressures need a lower temperature to foam and samples with longer desorption times need a higher temperature to foam to reach the same density. The relative density decreases as the foaming temperature increases. This trend is the same regardless of the saturation pressure, desorption time, and initial sheet thickness. However, for sheets

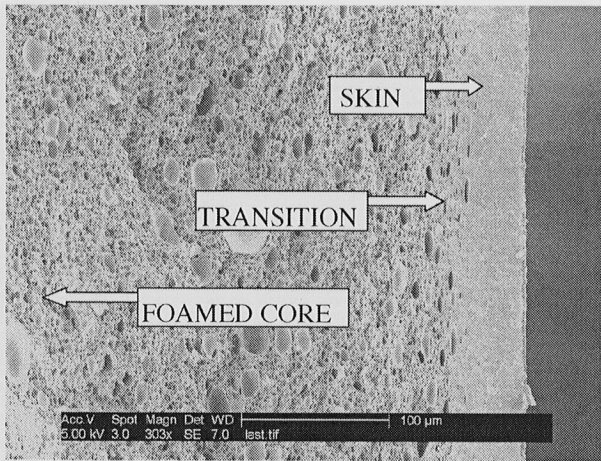


**Figure 7.** Relative density as a function of foaming temperature at various saturation and desorption conditions for initial sheet thickness 4.75 mm

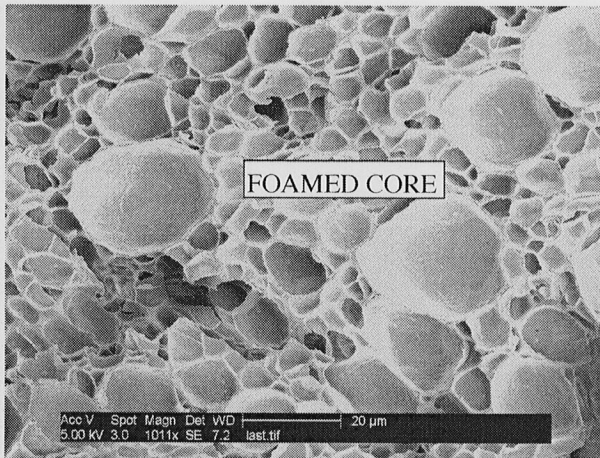
saturated at 3 MPa and 5 MPa as the foaming temperature increases to about 110 °C, it is observed that the rate at which the density decreases becomes slower. In cases where the foaming temperature is close to or above 116 °C, the  $T_g$  of the unsaturated ABS, the relative density increases with the foaming temperature. This could be due to the collapse of the foam structure.

### 4.3. Microstructure

Figure 8(a) shows an SEM image of the cross-sectional microstructure of a 13.5% relative density microcellular ABS sample that was saturated with CO<sub>2</sub> at 3 MPa, desorbed for 2 days and foamed at 112.5 °C. The initial thickness of the unfoamed sample was 9.53 mm. The image shows an integral skin of 50 μm thickness and foamed core with uniformly distributed microbubbles. Also, a transition region is visible between the integral skin and foamed core where the bubbles are elongated. This bubble elongation is a result of constraining the foam growth occurring in the thickness direction during the foaming process. Figure 8(b) shows a magnified image of the foamed core for the same sample. As seen the core consists of 15-20 μm bubbles interspersed among uniformly distributed microbubbles in the 3-5 μm range. Figures 9(a) and 9(b) show micrographs of the core and skin regions for a 39.8% relative density microcellular ABS sample processed at 1 MPa saturation pressure, 0 day desorption time and 130 °C



(a)



(b)

**Figure 8. (a) SEM of a 13.9% relative density ABS sample showing skin, transition area and core. The sample was saturated at 3 MPa, desorbed for 2 days at atmospheric conditions and was foamed in a hot press at 112.5 °C resulting in a skin thickness of 50 μm (b) SEM photo of the same sample core region at a higher magnification shows 15-20 μm bubbles interspersed among uniformly distributed 3-5 μm bubbles**

foaming temperature. The initial thickness was 9.53 mm. Similarly, Figures 9(c) and 9(d) show the core and skin regions of a 37.3% relative density ABS foam sample processed at 1 MPa saturation pressure, 2 days desorption time, 140 °C foaming temperature and initial thickness of 9.53 mm. Comparing Figures 9(b)

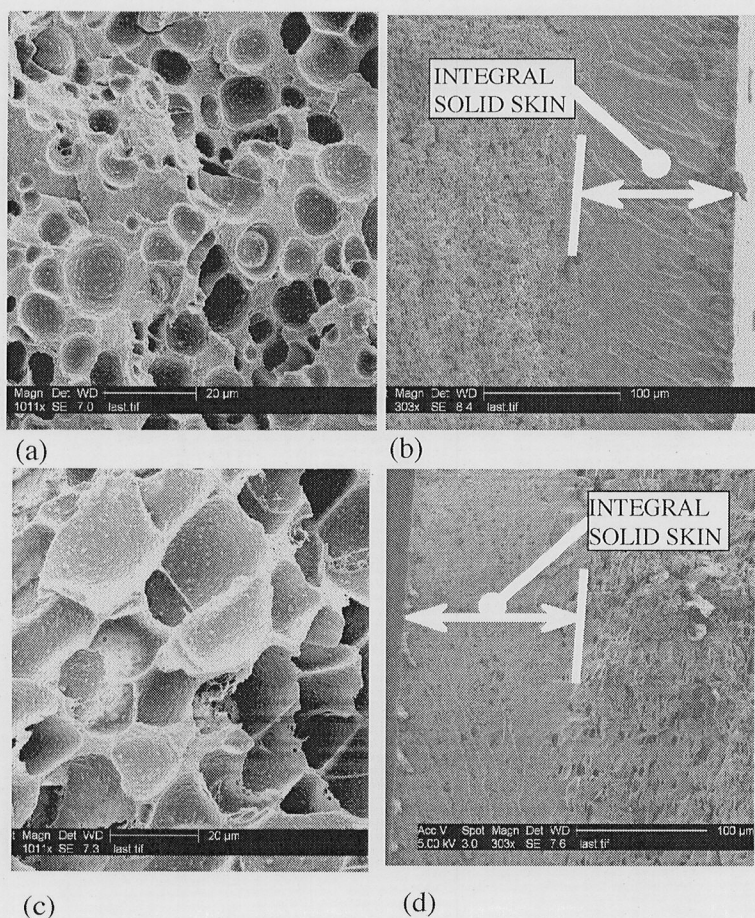


**Figure 9.** (a) SEM showing the core region of a 39.8% relative density microcellular ABS sample saturated with CO<sub>2</sub> at 1 MPa, desorbed for 0 day and foamed at 130 °C. (b) SEM of the same 39.8% relative density sample showing a 100 μm thick integral skin. (c) SEM showing the core region of a 37.3% relative density microcellular ABS sample saturated with CO<sub>2</sub> at 1 MPa, desorbed for 2 days and foamed at 140 °C. (d) SEM of the same 37.3% relative density sample showing a 140 μm integral skin. Note that as desorption time increases the thickness of the integral skin increases for foams of similar densities

and 9(d) it can be seen that as desorption time increases from 0 day to 2 days the skin thickness increases from 100 μm to 140 μm. Figures 9(a) and 9(c) show that for the same saturation pressure and similar density the average cell size increases as the foaming temperature increases. Similarly, Figures 10(b) and 10(d) show that, for the samples saturated at 5 MPa, the skin thickness increases

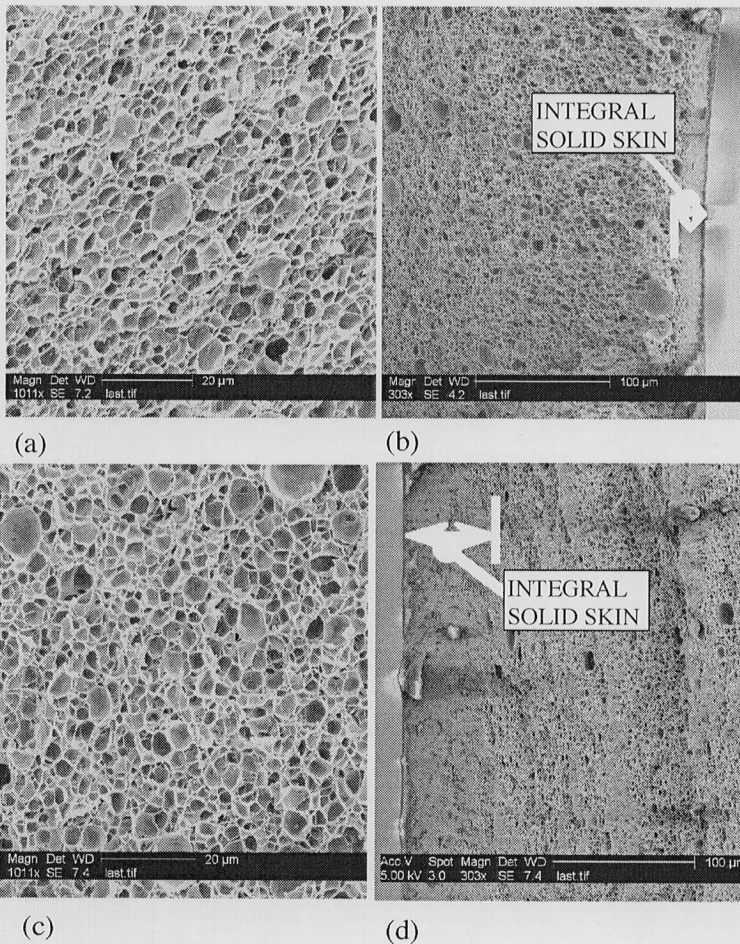


**Figure 10.** (a) SEM showing the core region of a 26.5% relative density microcellular ABS sample saturated with CO<sub>2</sub> at 5 MPa, desorbed for 0 day and foamed at 92.5 °C. (b) SEM of the same 26.5% relative density sample showing a 25 μm thick integral skin. (c) SEM showing the core region of a 22.8% relative density microcellular ABS sample saturated with CO<sub>2</sub> at 5 MPa, desorbed for 2 days and foamed at 102.5 °C. (d) SEM of the same 22.8% relative density sample showing a 50 μm integral skin. Note that as desorption time increases the thickness of the integral skin increases for foams of similar densities

from 25 μm to 50 μm as the desorption time increases from 0 day to 2 days. These results show that for similar density foams the skin thickness can be easily controlled by using desorption time as a process variable. It can be seen from the comparison of Figures 9(a)-(d) with Figures 10(a)-(d), that as the saturation pressure increases the cell density increases and the cell size decreases. This can

be attributed to the higher nucleation density resulting from the use of higher saturation pressures<sup>(15)</sup>.

#### 4.4. Process Model

A screening analysis was conducted on the relative density of the microcellular ABS samples. This was done to determine the relative significance of various factors in the constrained foaming experiments. In the analysis, the factors examined were the linear effects of all the variables, quadratic effects of the variables that had more than two levels, cubic and fourth-order effects of the variables that had more than four levels and the second order interaction effects of all the variables. Figure 11 shows a Pareto chart of the orthogonal estimates of all the effects. This chart plots the composition of the absolute values of the normalized estimates relative to the sum of these values. A cumulative line shows the advance to 100% of the sum of absolute values. The Pareto chart reveals the relative significance among the factors examined. From Figure 11, it can be seen that the linear effect of foaming temperature is the most significant, followed by the interaction effect of foaming temperature and saturation pressure, the interaction effect of foaming temperature and desorption time, the interaction effect of saturation pressure and starting thickness, the interaction effect of saturation pressure and desorption time, quadratic effect of saturation pressure, the cubic effect of foaming temperature, and so on. A

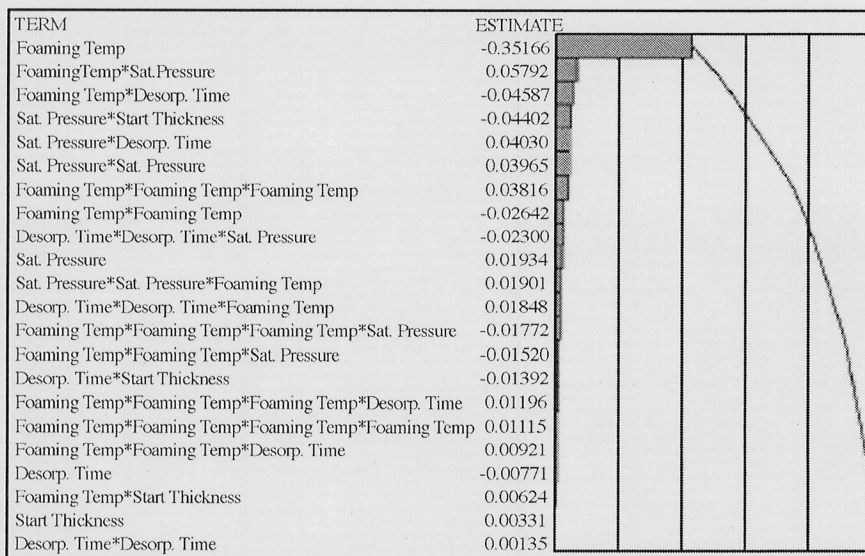


Figure 11. Pareto chart of estimated effects



forward stepwise regression with 25% probability to enter and 10% probability to leave yields a response model of the relative density as follows. The model has an adjusted R<sup>2</sup> value of 94.22%.

$$\rho_{rel} = 0.5287 - 0.35166 * T_{foam} + 0.05792 * T_{foam} * P_{sat} - 0.04587 * T_{foam} * t_d - 0.04402 * P_{sat} * h + 0.0403 * P_{sat} * t_d + 0.03965 * P_{sat}^2 + 0.03816 * T_{foam}^3 - 0.02642 * T_{foam}^2 - 0.023 * t_d^2 * P_{sat} + 0.01934 * P_{sat} + 0.01901 * P_{sat}^2 * T_{foam} + 0.01848 * t_d^2 * T_{foam} - 0.01772 * T_{foam}^3 * P_{sat} - 0.0152 * T_{foam}^2 * P_{sat} - 0.01392 * t_d * h + 0.01196 * T_{foam}^3 * t_d + 0.01115 * T_{foam}^4 + 0.00921 * T_{foam}^2 * t_d - 0.00771 * t_d + 0.00624 * T_{foam} * h + 0.00331 * h + 0.00135 * t_d^2 \quad (1)$$

Observations suggest that samples with high gas concentration (because of high saturation pressure) need a lower temperature to foam, and thus if the samples are foamed at a high temperature, very low density can be achieved. However, high gas concentration does not always guarantee low density foams. From the model in Equation (1), it is found that the lowest relative density of 14.1% is achieved by setting the saturation pressure at 5 MPa, desorption time at 0 day, starting thickness 9.53 mm and the foaming temperature at 110 °C. However, at these conditions experimental data shows that the relative density achieved is 26.8%. Experimentally the lowest relative density of 9.6% was achieved at a saturation pressure of 3 MPa, desorption time of 1 day, starting thickness of 4.75 mm and a foaming temperature of 125 °C. At these conditions the model represented by Equation (1) predicts a relative density of 18.8%.

The discrepancy between the lowest relative density predicted by the model and that resulting from the experiment can be explained as follows. In Figures 6 and 7, the general trend is that the relative density decreases with increasing foaming temperature until a minimum relative density is reached after which any further increase in foaming temperature has the effect of increasing the relative density. This is due to the collapse of the bubble structure in the core of the thick microcellular sheets. However, for curves representing 5 MPa saturation, 0 day desorption and 5 MPa saturation, 1 day desorption conditions, the trend of relative density decreasing with foaming temperature could only be captured at the foaming temperatures that were studied. This is the reason the regression model in equation (1) could not predict the lowest relative density at the same process conditions as the experiment. More experimentation around the lowest relative densities is needed to capture the trend where the relative density increases with foaming temperature due to bubble collapse. This would improve the regression model given by equation (1) to predict much closely the experimental results at conditions where the bubble collapse occurs. In general, the response model yields satisfactory predictions at other foaming conditions.

## 5. SUMMARY

The batch microcellular process was scaled up to produce microcellular panels from PMMA, PS and ABS of varying thicknesses. The feasibility to produce microcellular panels with reduced density over a wide range was established. For the ABS-CO<sub>2</sub> system, a detailed design of experiments study was conducted which showed that density reductions of up to 92% can be achieved with integral skins of desired thickness. Also, a regression model based on the results of the design of experiments study reveals that foaming temperature and the first order interaction of foaming temperature with desorption time and gas saturation pressure have the predominant effect on the foam density.

The thick solid-state microcellular panels can be integrated into advanced panel systems providing light weight and energy efficient materials for construction. The idea of constrained foaming to produce flat microcellular panels can be easily extended to produce contoured shapes by foaming a sheet between the walls of a heated mold. Thus one can envision many applications of microcellular panels such as in automotive and transportation industries.

## ACKNOWLEDGEMENTS

The authors wish to acknowledge the National Science Foundation of the USA for financial support under Grant No. CMS-0122055.

## REFERENCES

1. Martini J. Waldman F. A., and Suh N. P., (1982), "The Production and Analysis of Microcellular Foam," *SPE Tech. Papers: XXVIII*, pp. 674-676
2. Kumar V., (1993), "Microcellular Polymers: Novel Materials for the 21st Century," *Progress in Rubber and Plastics Technology*, Vol. 9, No. 1, pp. 54-70.
3. Kumar V., VanderWel M., Weller J. E., and Seeler K. A., (1994), "Experimental Characterization of the Tensile Behavior of Microcellular Polycarbonate Foams," *Journal of Engineering Materials and Technology*, Vol. 116, pp. 439-445.
4. Seeler K. A and Kumar V., (1993), "Tension-Tension Fatigue of Microcellular Polycarbonate: Initial Results," *Journal of Reinforced Plastics and Composites*, Vol. 12, No. 3, pp. 359-376.
5. Barlow C., Kumar V., Flinn B., Bordia R. K., and Weller J. E., (2001), "Impact Strength of High Density Solid-State Microcellular Polycarbonate Foams," *Journal of Engineering Materials and Technology*, Vol. 123, pp. 229-233.

6. Collias D. I., and Baird D. G., (1994), "Impact toughening of polycarbonate by microcellular foaming," *Polymer*, Volume 35, Issue 18, September 1994, pp. 3978-3983.
7. Kumar V., Juntunen R. P., and Barlow C., (2000), "Impact Strength of High Relative Density Solid State Carbon Dioxide Blown Crystallizable Poly(Ethylene Terephthalate) Microcellular Foams," *Cellular Polymers*, Vol. 19, No. 1, pp.25-37.
8. Juntunen R. P., Kumar V., and Weller J. E., (2000), "Impact Strength of High Density Microcellular Poly(Vinyl Chloride) Foams," *Journal of Vinyl and Additive Technology*, Vol. 6, No. 2, pp. 93-99.
9. Kumar V., Fidale T., Nix K., and Juntunen R., (2000), "Thermal Conductivity of High Density CPET Microcellular Foams," *FOAMS 2000 – Second International Conference*, Parsippany, NJ, October 24-25, Society of Plastics Engineers, pp. 117-126.
10. Zhang Z., and Handa Y. P., (1998), "An In-Situ Study of Plasticization of Polymers by High-Pressure Gases," *Journal of Polymer Science: Part B - Polymer Physics*, Vol. 36, pp. 977-982.
11. Kumar V. and Weller J.E., (1994), "A Model for the Un-foamed Skin on Microcellular Foams," *Polymer Engineering and Science*, Vol. 34, pp. 169-173.
12. Baldwin D. F., Park C. B., and Suh N. M., (1996), "An Extrusion System for the Processing of Microcellular Polymer Sheets: Shaping and Cell Growth," *Polymer Engineering and Science*, Vol. 36, No. 10, pp. 1425-1435.
13. Baldwin D. F., Park C. B., and Suh N. M., (1998), "Microcellular Sheet Extrusion System Process Design Models for Shaping and Cell Growth Control," *Polymer Engineering and Science*, Vol. 38, No. 4, pp. 674-688.
14. Kumar V., Nadella K., and Li W., (2003), "Production of Thick Microcellular Thermoplastic Sheets," *ANTEC 2003- Proceedings of the 61st Annual Technical Conference & Exhibition*, Vol. XLIX, Nashville, TN, April 27-May 2, Society of Plastics Engineers, pp. 1722-1726.
15. Kumar V., and Weller J. E., (1994), "Production of Microcellular Polycarbonate Using Carbon Dioxide for Bubble Nucleation," *Journal of Engineering for Industry*, Vol. 116, pp. 413-420.
16. Kumar V., Weller J. E., and Montecillo R., (1992), "Microcellular PVC," *Journal of Vinyl Technology*, Vol.14, No. 4, pp. 191-197.
17. Murray, R. E., Weller, J. E. and Kumar V., (2000), "Solid-State Microcellular Acrylonitrile-Butadiene-Styrene Foams," *Cellular Polymers*, Vol. 19, No. 6, pp. 413-426.

18. Li, W., Cheng, S.W., Hu, S.J., and Shriver, J., (2001), "Statistical Investigation on Resistance Spot Welding Quality using a Two-stage, Sliding-level Experiment." *ASME Transaction Journal of Manufacturing Science and Engineering*, Vol. 123, pp. 513-520.
19. Chow, T. S., (1980), "Molecular Interpretation of the Glass Transition Temperature of Polymer-Diluent Systems," *Macromolecules*, Vol. 13, pp. 362-364.
20. ASTM D-792, *Standard Test Methods for Density and Specific Gravity (relative density) of Plastics by Displacement*, ASTM International, West Conshohocken, PA, 2002.